ARTICLES

Conformational Dynamics of Semiflexibly Bridged Donor−Acceptor Systems Studied with a Streak Camera and Spectrotemporal Parametrization of Fluorescence

Xavier Y. Lauteslager,[†] Ivo H. M. van Stokkum,[‡] Hendrik J. van Ramesdonk,[†] Albert M. Brouwer,*[,†] and Jan W. Verhoeven[†]

Institute of Molecular Chemistry, University of Amsterdam, Nieuwe Achtergracht 129, NL-1018 WS Amsterdam, The Netherlands, and Division of Physics and Astronomy, Faculty of Sciences, Vrije Universiteit Amsterdam, De Boelelaan 1081, NL-1081 HV Amsterdam, The Netherlands

Received: September 3, 1998

The fluorescence of four semiflexibly bridged donor−bridge−acceptor systems was studied with a streak camera system. The information-rich streak data make a detailed analysis possible of both the kinetics and the spectral changes that take place. From the analysis, it follows that all compounds studied undergo a photoinduced harpooning process in which long-range electron transfer creates an extended charge-transfer (ECT) species, which converts to a compact charge-transfer (CCT) species due to Coulombic attraction. Both the ECT and CCT species display CT fluorescence. The harpooning process occurs even in solvents of medium polarity (e.g., diethyl ether), whereas it has previously been assumed for related compounds that this process only occurs in the gas phase and in nonpolar alkane solvents.

1. Introduction

Recently, we have reported the synthesis of the new "harpooning" systems **1**−**3** (Chart 1).[1] As in compound **4**, which we studied earlier,[2] exciplex-like compact charge-transfer (CCT) species with the bridging piperidine ring in a (twist) boat conformation are formed in these compounds from extended charge-transfer (ECT) species in which the donor and acceptor are well separated in space. The formation of the ECT species involves a charge-transfer process in which the molecule is still in an extended conformation similar to the ground-state structure, with the piperidine ring in the preferred chair conformation. Crucial for the observation of this harpooning process (Scheme 1) is the fact that the ECT state and the CCT state both show radiative decay. The compounds **1**−**4** have virtually identical energies of their locally excited states, and also the energies of their CT excited states are very similar. They differ only in the presence or absence of long alkyl chains, which makes them ideally suited for probing hydrodynamic (viscosity) effects on the harpooning process.

The compounds were studied previously by a combination of steady-state and time-resolved fluorescence, supplemented by time-resolved microwave conductivity measurements (TRMC).[1] In these studies, the conversion of the ECT into the CCT species could only be detected convincingly in the nonpolar alkane solvents. In the more polar dialkyl ether solvents, biexponential fluorescence decay pointed to the presence of two species as well but extensive spectral overlap prevented a full analysis by the methods used. The analysis of the solvent dependence of the steady-state fluorescence maxima also provided some indication that the harpooning process might still take place in relatively polar solvents such as diethyl ether. However, such an analysis is rather tricky if the fluorescence maxima are derived from steady-state spectra, which show a superposition of the ECT and CCT emission bands.

We now present the results of a multiwavelength time-resolved fluorescence study performed with a streak camera system. The streak images obtained were analyzed by the

CHART 1

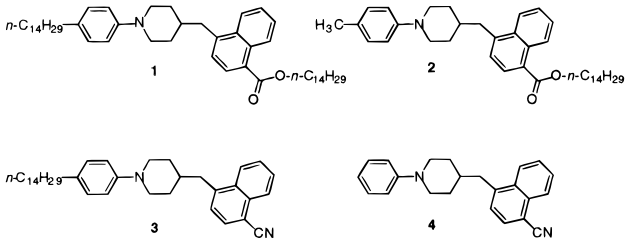

SCHEME 1. Schematic Representation of the Harpooning Mechanism

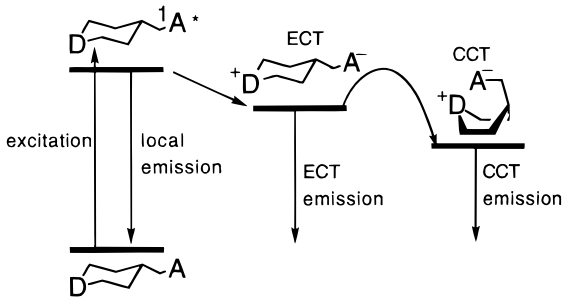

* Author to whom correspondence should be addressed. Fax: 31 20 525 5670. E-mail: fred@org.chem.uva.nl.
† University of Amsterdam.
‡ Vrije Universiteit Amsterdam.

10.1021/jp983595h CCC: $18.00
Published on Web 01/22/1999

method of spectrotemporal parametrization of fluorescence (section 2). The compounds investigated are the above-mentioned systems **1**−**3**, as well as **4** (Chart 1), the first donor−acceptor system in which the harpooning mechanism was proven to occur.[2] We will show that the combination of the information-rich streak images with analysis by spectrotemporal parametrization of the fluorescence data is ideally suited to study the conformational dynamics of the harpooning systems and enables us to study the fluorescence kinetics in greater detail even at room temperature, at which the processes are relatively fast.

2. Spectrotemporal Parametrization of Fluorescence

Several cases have been studied in our laboratory in which the dynamics of fluorescence could be employed to monitor conformational changes (in particular upon harpooning) in semirigidly bridged donor−acceptor systems.[3−5] This was mainly done by applying kinetic models and spectral models to sets of nanosecond time-resolved fluorescence data obtained using a time-gated optical multichannel analyzer, which provides high spectral resolution.[3] The disadvantage of this method is the low time resolution, which could be overcome by complementing these data with fluorescence decays measured with higher time resolution at a small number (typically 12) of wavelengths.[4] Furthermore, for some compounds, the influence of temperature and solvent viscosity on the folding process from an ECT to a CCT species in nonpolar alkane solvents was studied.[5]

We will now briefly describe the method of spectrotemporal parametrization. For a more detailed description, the reader is referred to van Stokkum et al.[3,4] By means of time-resolved spectroscopy, the kinetics of a mixture of components whose spectra overlap can be measured indirectly by observing the total spectrum as a function of time. The perfect, noise-free, time-resolved spectrum Ψ is a superposition of the contributions of the n_{comp} different components.

$$\Psi(t, \lambda) = \sum_{l=1}^{n_{comp}} c_l(t)\epsilon_l(\lambda) \qquad (1)$$

where $c_l(t)$ and $\epsilon_l(\lambda)$ denote, respectively, the concentration and emission spectrum of component l. Measurement of Ψ poses the inverse problem, how can the spectroscopic and kinetic properties of the components be recovered? The first task to be performed is to determine the number of components from the data by singular value decomposition (SVD). The next step is to estimate the kinetic parameters using a compartmental model[6] (i.e., a model with differential equations that are linear in the concentrations, like first-order chemical reactions) and estimate the parameters that describe the spectra. The results of the parameter estimation consist of a kinetic model with estimated rate constants as well as the (shapes of the) emission spectra of the components.

The shape of a charge-transfer fluorescence emission spectrum is often well described by a Gaussian in the energy domain $f(\nu)/\nu^3 = f_{max} \exp(-\ln 2[2(\nu - \nu_{max})/\Delta\nu]^2)$, where $\nu = \lambda^{-1}$ denotes the wavenumber and $f(\nu)$ is the converted fluorescence emission spectrum, $f(\nu) = \lambda^2\epsilon(\lambda)$.[7] The Franck−Condon wavenumber of maximum emission is denoted by ν_{max}, whereas $\Delta\nu$ is the full width at half-maximum. Even better fits are achieved when an extra skewness parameter is introduced.[8] Thus, we arrive at the model function

$$\epsilon(\nu) = \nu^5 f_{max} \exp(-\ln 2[\ln(1 + 2b(\nu - \nu_{max})/\Delta\nu)/b]^2) \qquad (2)$$

Note that with the skewness parameter $b \rightarrow 0$ the exponent in eq 2 reduces to a Gaussian. The shape described by the model function (2) is indistinguishable from the spectral shape predicted for CT-type emission bands.[9] Below, we will consider simple two-compartment models: (1) a parallel model which is appropriate for two independently decaying components, leading to decay associated spectra (DAS) or (2) a sequential model for two interconverting species as occurs in the harpooning mechanism, giving species associated spectra (SAS).

The quality of the fit, as indicated by the residuals and root-mean-square error (rmse), depends only on the number of compartments and not on the type of model. Also, the estimated rate constants are identical with a parallel or sequential model. However, the DAS and SAS of the first component are different, which allows the appropriate model to be chosen.

3. Results and Discussion

3.1. Analysis of the Harpooning Systems. For the four donor−acceptor systems, streak images were measured in nine solvents. It is important to stress that in none of the solvents do any of the four systems display significant local donor or acceptor fluorescence, as is obvious from the absence of fluorescence bands below 360 nm.[1] Thus, in all cases, photoexcitation must be followed by very fast intramolecular charge separation and solvent relaxation[10] on a time scale ($\geq 10^{11}$ s^{-1}) much faster than that of the harpooning process.

We will describe in detail the results of the spectrotemporal parametrization method for **4** (the "old" harpooning system) and **1** (the harpooning system with a tetradecyl chain attached to both donor and acceptor) in two solvents (*trans*-decalin and diethyl ether). The results of the other compounds and solvents will be presented more briefly. In the alkane solvents, two time windows were chosen in order to accurately determine the lifetime of both the ECT and CCT species.

In all nonpolar solvents, the matrix of streak data gives rise to two pairs of singular vectors and two singular values significantly different from noise (not shown). This implies that two spectrally and temporally different components are present, as expected. In Figure 1, we present decay traces in *trans*-decalin for **4** and **1** at wavelengths close to the expected maxima of the ECT (Figure 1A,B) and CCT species (Figure 1C,D). The decays shown in parts A and B of Figure 1 are fast and monoexponential. Clearly, the decay time of the ECT species of **4** (2.0 ns) is much shorter than that of **1** (9.4 ns). In parts C and D of Figure 1, we observe a fast rise (solid line) followed by a slow decay (dotted line). The decay (DAS) and species (SAS) associated spectra of **4** and **1** in *trans*-decalin are shown in Figure 2.

The data could well be fitted with the sequential model in which the slow-decaying redmost component (dotted line, 70 ns for **4** and 36 ns for **1**) is formed from the fast-decaying component. This is illustrated by the negative amplitudes of the first DAS (full line) at wavelengths greater than 420 nm for **4** (2.0 ns, Figure 2A) and greater than 440 nm for **1** (9.4 ns, Figure 2B) for the fast-decaying component. This is in line with the harpooning mechanism in which the blue emission of the first SAS (full line in Figure 2C,D) stems from a primarily formed extended charge-transfer (ECT) species that is converted into a folded or compact charge-transfer (CCT) species emitting at longer wavelength. From the SAS, we can determine the ν_{max} (by applying a fit of the spectral shape to eq 2) of the two species, which amount to 25.6×10^3 and 21.5×10^3 cm^{-1} for **4** (Figure 2C) and 24.2×10^3 and 20.2×10^3 cm^{-1} for **1** (Figure 2D).

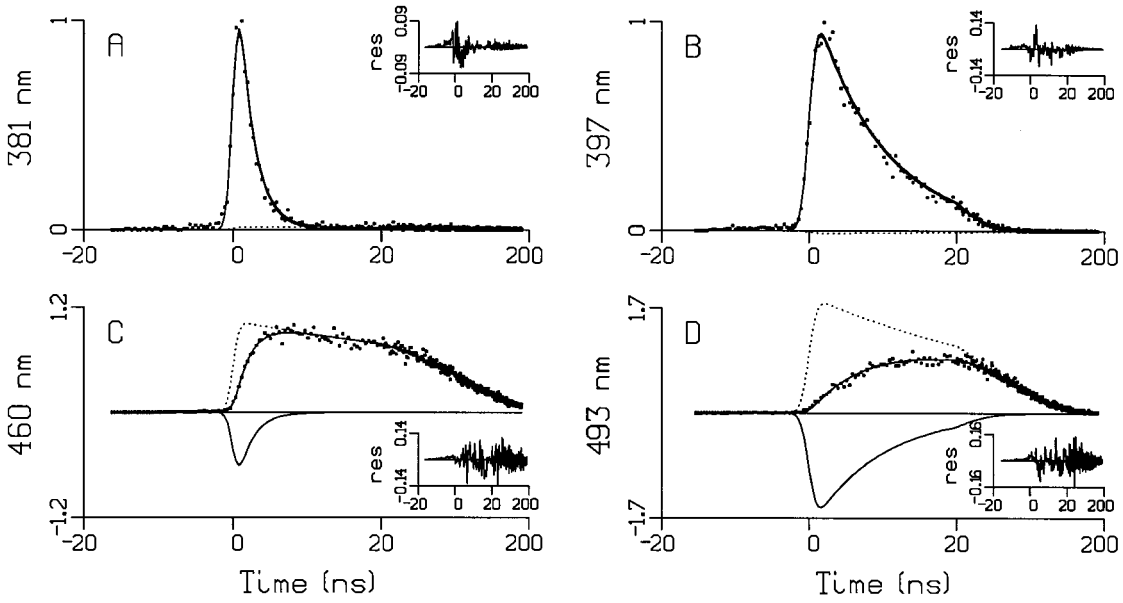

Figure 1. Results from global analysis of (normalized) kinetics in **4** (A and C) and **1** (B and D) in *trans*-decalin at representative wavelengths (see labels at the vertical axes). Insets show residuals of a fit with two monoexponential decays. The contributions of the decays to the fit are depicted by different line styles. 2.0 ns (solid in A and C); 70 ns (dotted in A and C); 9.4 ns (solid in B and D); 36 ns (dotted in B and D). The sum of the contributions is represented by a solid line through the measured points. The time base from −20 to +20 ns (relative to the maximum of the instrument response) is linear, and from 20 to 200 ns it is logarithmic.

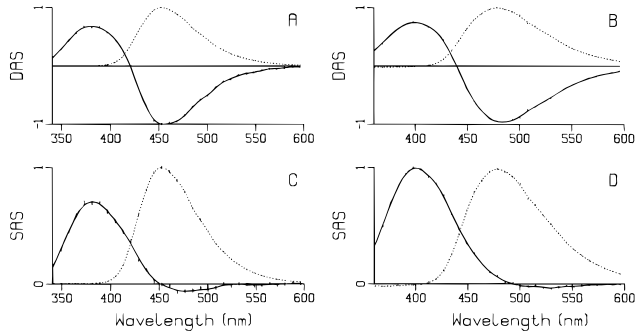

Figure 2. Decay and species associated spectra of **4** (A and C) and **1** (B and D) in *trans*-decalin. Vertical lines indicate plus or minus standard error in amplitude: 2.0 ns (solid in A and C); 70 ns (dotted in A and C); 9.4 ns (solid in B and D); 36 ns (dotted in B and D). Note that the second SAS plotted here is in fact the product of the quantum yield of folding and the true SAS of the CCT state.

4 and **1** show similar behavior in the other alkane solvents, as do **2** and **3**. As we go from the alkane solvents to the more polar solvent di-*n*-pentyl ether, we observe a red shift of both the ECT and CCT emission spectra, as expected for charge-separated states. The red shift of the emission of the ECT species, however, is larger as it becomes relatively more stabilized due to the larger dipole moment compared to that of the CCT species. As a result, the overlap of the species associated spectra increases upon increasing the solvent polarity. For **4**, the kinetics of fluorescence have previously not been studied in great detail in solvents more polar than the saturated hydrocarbons. Because for structurally related compounds no folding was observed[4] in solvents other than alkanes, it was assumed that for **4** as well the CCT species is only formed in the saturated hydrocarbon solvents.[2] The analysis of the streak images presented here clearly proves that this assumption is invalid. Decay traces given in Figure 3 show that even in solvents as polar as diethyl ether a rise is observed on the low-energy side of the emission band with a time constant of 5.9 ns for **4** and 8.8 ns for **1**, followed by a slow decay (27 ns for **4** and 25 ns for **1**).

Upon analysis of the streak images in the ether solvents, we indeed find two pairs of singular vectors and two singular values significantly different from noise, as in the alkane solvents. Again, the two compartment model can perfectly fit the data. In the DAS (Figure 4A, B), the spectrum belonging to the moderately fast decaying species (full line) shows negative amplitudes, as it is the precursor of the slow-decaying species. In Figure 4C,D, we present the SAS for **4** and **1** in diethyl ether. We observe two largely overlapping spectra with virtually identical ν_{max} (19.8×10^3 and 19.7×10^3 cm^{-1} for **4** and 19.1×10^3 and 18.8×10^3 cm^{-1} for **1**). A model with a single component yields unsatisfactory results, as can be concluded from the structured residuals and the increase of the rmse by 7% (**4**) and 14% (**1**).

The fact that the difference between the Franck−Condon maxima of the ECT and CCT species in diethyl ether is very small is not in line with the potential energy scheme that is usually drawn for the harpooning mechanism to explain the observed dual emission bands in nonpolar alkane solvents. In this scheme (Figure 5, left-hand diagram), the emission maximum of the CCT species is red-shifted compared to that of the ECT species because of two factors. First, the CCT species is assumed to be lower in energy because there exists a significant electrostatic driving force for the folding process to occur in these nonpolar solvents. Second, the nonrelaxed Franck−Condon ground state of the CCT species is assumed to be higher in energy compared to that of the ECT species because the former species returns to the ground state in the (twist) boat conformation, which is energetically unfavorable. The energy difference between the chair and (twist) boat conformation in the ground state is estimated to be ca. 5.5 kcal mol^{-1}, in analogy to the energy difference for the chair and (twist) boat conformation of cyclohexane.[11]

The left-hand diagram in Figure 5, however, does not take into account the difference in solvent reorganization energies between the ECT and CCT species, which gains importance upon increasing the solvent polarity. In contrast to the internal reorganization energy, the solvent reorganization energy of the

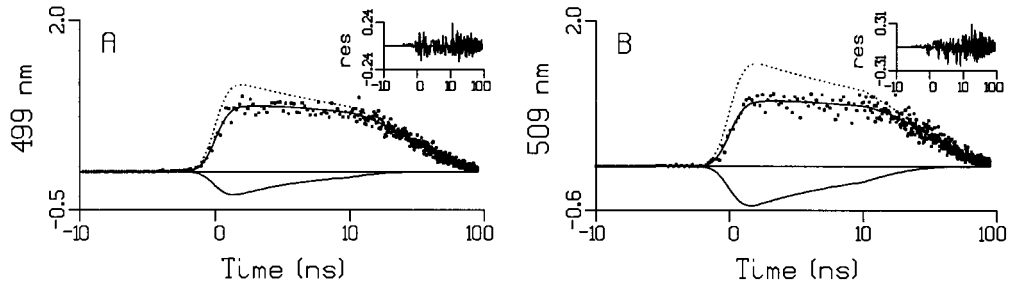

Figure 3. Results from global analysis of (normalized) kinetics in **4** (A) and **1** (B) in diethyl ether at representative wavelengths (see labels at the vertical axes). Insets show residuals of a fit with two monoexponential decays. The contributions of the decays to the fit are depicted by different line styles: 5.9 ns (solid in A); 27 ns (dotted in A); 8.8 ns (solid in B); 25 ns (dotted in B). The sum of the contributions is represented by a solid line through the measured points. The time base from −10 to +10 ns (relative to the maximum of the instrument response) is linear, and from 10 to 100 ns it is logarithmic.

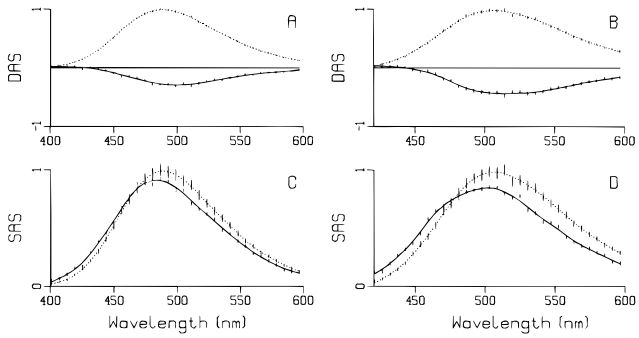

Figure 4. Decay and species associated spectra of **4** (A and C) and **1** (B and D) in diethyl ether. Vertical lines indicate plus or minus standard error in amplitude: 5.9 ns (solid in A and C); 27 ns (dotted in A and C); 8.8 ns (solid in B and D); 25 ns (dotted in B and D). Note that the second SAS plotted here is in fact the product of the quantum yield of folding and the true SAS of the CCT state.

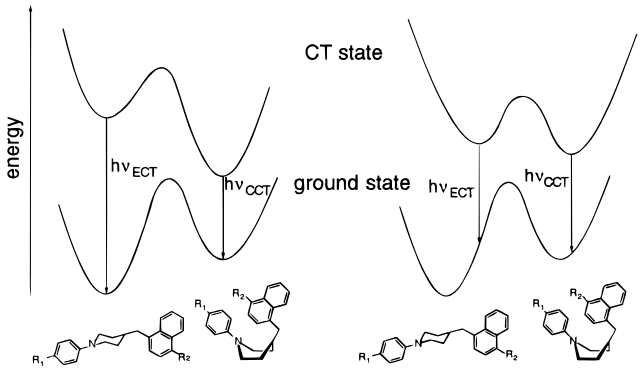

Figure 5. Potential energy schemes for the harpooning process in nonpolar alkane (left) and medium polar ether solvents (right). A schematic drawing of the nonrelaxed Franck−Condon ground states of the extended and folded species is also shown.

ECT species is expected to be significantly larger than that of the CCT species. Using the experimentally derived slopes of the Lippert−Mataga plots (vide infra), the solvent reorganization energy in diethyl ether of the ECT and CCT species can be calculated according to eq 3.[12]

$$\lambda_s = \frac{\mu^2}{\rho^3}\left(\frac{\epsilon_s - 1}{2\epsilon_s + 1} - \frac{n^2 - 1}{2n^2 + 1}\right) \qquad (3)$$

Using this formula, the solvent reorganization energy of the ECT species is calculated to be ca. 2×10^3 cm^{-1} (≈5.7 kcal mol^{-1}) larger than that of the CCT species. This roughly compensates the estimated energy difference of 5.5 kcal mol^{-1} between the two nonrelaxed ground states! Furthermore, the energy difference between the ECT and CCT species is expected to become less upon increasing the solvent polarity, because of the diminishing influence of the Coulomb attraction. Taking the factors described above into account, we can sketch the potential energy scheme as given in the right-hand diagram of Figure 5.

TABLE 1: Estimated ECT and CCT Lifetimes (ns) for 1−4 in Various Solvents

	1		**2**		**3**		**4**	
solvent	τ_{ECT}	τ_{CCT}	τ_{ECT}	τ_{CCT}	τ_{ECT}	τ_{CCT}	τ_{ECT}	τ_{CCT}
n-hexane	1.2	24.2	1.4	24.4	<1	35.2	<1	40.7
cyclohexane	3.1	27.0	1.8	27.1	1.3	44.2	0.6	40.7
trans-decalin	9.4	36.2	4.1	34.1	3.9	59.3	2.0	70.0
di-*n*-pentyl ether	10.8	24.1	8.5	21.6	8.4	35.8	6.7	35.9
benzene	7.9	33.9	6.3	29.9	6.1	42.5	5.4	39.1
diisopropyl ether	5.9	17.5	6.6	17.0	7.5	20.9	5.2	12.8
diethyl ether	8.8	25.2	7.0	24.0	7.5	25.9	5.9	26.6
ethyl acetate	9.9[a]		6.1[a]		21.4		25.1	
tetrahydrofuran	16.1[a]		11.7[a]		33.2		33.7	

[a] Minor short-lived component observed as well.

TABLE 2: Decay Rates (10^9 s^{-1}) of the ECT Species of 1−4 in Solvents in which Harpooning Is Observed[a]

solvent	η (cP)	ϵ_s	**1**	**2**	**3**	**4**
n-hexane	0.31	1.89	0.83	0.69	>1	>1
cyclohexane	0.98	2.02	0.32	0.57	0.76	1.59
trans-decalin	2.13	2.17	0.11	0.24	0.26	0.50
diethyl ether	0.23	4.34	0.11	0.14	0.13	0.17
diisopropyl ether	0.33	3.98	0.17	0.15	0.13	0.19
benzene	0.65	2.28	0.13	0.16	0.16	0.19
di-*n*-pentyl ether	1.08	2.77	0.093	0.12	0.087	0.15

[a] Viscosity η and dielectric constant ϵ_s are included for reference.

Considering this potential energy scheme, an equilibrium situation between the ECT and CCT species might be more appropriate to describe the kinetics and spectral changes, especially in more polar solvents. A compartmental model with an equilibrium between the ECT and CCT species requires an extra rate constant that cannot be estimated from the data. To see which effect this equilibrium would have on the SAS, we fixed the rate $k_{CCT\rightarrow ECT}$ to a trial value of 0.015×10^9 s^{-1} for **4** in diethyl ether. This also resulted in satisfactory SAS, only slightly different from those in Figure 4C. Thus, an equilibrium cannot be excluded a priori based on SAS. For simplicity, we restrict ourselves here to the sequential model. In ethyl acetate and tetrahydrofuran, the single component model yields satisfactory results. Presumably, in these solvents the harpooning process does not occur (for **1** and **2**, a minor short-lived component is observed as well, with an identically shaped DAS).

The analysis, presented above for **4** and **1** in *trans*-decalin and diethyl ether, was performed for all compounds in nine

TABLE 3: Franck−Condon Emission Maxima (ν_{max} 10^3 cm^{-1}) of the ECT and CCT Species of 1−4 in Various Solvents

		1		2		3		4	
solvent	Δf[a]	ECT	CCT	ECT	CCT	ECT	CCT	ECT	CCT
n-hexane	0.092	24.7	20.6	23.9	20.5	25.1	21.0	25.8	21.9
cyclohexane	0.100	24.5	20.3	23.9	20.4	24.7	20.9	25.2	21.8
trans-decalin	0.110	24.2	20.2	23.6	20.3	24.4	20.6	25.6	21.5
di-*n*-pentyl ether	0.171	21.8	20.2	20.9	19.4	20.8	19.7	21.4	20.5
benzene	0.116[b]	20.3	18.9	20.1	18.9	20.2	19.0	20.9	19.9
diisopropyl ether	0.237	19.6	18.9	19.4	18.9	19.4	19.1	20.0	19.8
diethyl ether	0.251	19.1	18.8	19.0	18.8	19.0	18.9	19.8	19.7
ethyl acetate	0.292	16.8		16.7		16.6		17.3	
tetrahydrofuran	0.308	16.9		16.8		16.7		17.4	

[a] See equation 6. [b] Benzene is known to behave as more polar than expected based on its Δf value (ref 10).

solvents. The lifetimes obtained for the ECT and CCT (in case of alkane and ether solvents) species are given in Table 1.

Clear trends in the ECT lifetimes can be observed in those solvents in which harpooning occurs. Except for in *n*-hexane and diisopropyl ether, the ECT lifetimes of **1** are significantly longer than those of the other systems. The similarities in the CCT lifetimes of **1** and **2** on one side and **3** and **4** on the other are striking. Both **1** and **2** incorporate the same naphthalene ester acceptor chromophore, whereas **3** and **4** possess the same cyanonaphthalene acceptor chromophore. This indicates that the CCT lifetimes are largely determined by the acceptor chromophore incorporated.

The decay rates of the ECT species in those solvents in which harpooning occurs are given in Table 2, together with the viscosities and permittivities of the solvents used.

The decay rate of the ECT species approximates the rate of folding when the latter is much larger than the sum of the other radiative and nonradiative decay rates of the ECT species (eq 4).

$$k^{ECT} = k_f^{ECT} + k_d^{ECT} + k_{fold} \quad (4)$$

The term ($k_f^{ECT} + k_d^{ECT}$) in eq 4 represents the inverse lifetime of the extended charge-transfer state in the absence of the folding process. In the alkane solvents, a decrease of the ECT decay rate can be observed upon increasing the solvent viscosity. The effect of viscosity is most pronounced for **1**, which has long alkyl tails attached to both the donor and acceptor chromophore. The compounds with only one alkyl tail, **2** and **3**, show decay rates between those of **1** and **4**. For the other solvents, no clear trends are apparent. The reason is probably 2-fold. First, the assumption that the rate of folding can be approximated by the inverse of the ECT lifetime is probably not correct in these solvents as the ECT decay time is significantly longer in these solvents. Second, whereas the solvent dielectric permittivity in the alkane solvents is nearly constant (2.0 ± 10%), in the ether solvents, it varies from 2.77 (di-*n*-pentyl ether) to 4.34 (diethyl ether). We have shown before that the photoinduced harpooning process is strongly influenced by variations in the solvent permittivity.[13]

The method of spectrotemporal parametrization also yields the (shapes of the) emission spectra of the species as shown above. This enables us to investigate solvatochromic shifts as a function of the solvent polarity. In Table 3, we present the Franck−Condon maxima (in cm^{-1}, as derived from a fit of the band shape to eq 2; for more details, see the Supporting Information, Tables S1−S4) of the ECT and CCT (when formed) species in the solvents investigated. Knowing the maxima of both ECT and CCT species we can apply the well-known Lippert−Mataga analysis,[14] in which the solvent dependence of the charge-transfer emission wavenumber ν_{CT} is correlated with the solvent polarity parameter Δf according to eq 5, where $\nu_{CT}(0)$ (in cm^{-1}) is the emission maximum in the gas phase, μ_{CT} (in Debye) is the dipole moment of the charge-transfer state, h is Planck's constant, c is the velocity of light, ρ (in Å) is the effective radius of the solvent cavity occupied by the molecule, and Δf is defined by eq 6, in which ϵ_s is the solvent dielectric constant and n is its refractive index.

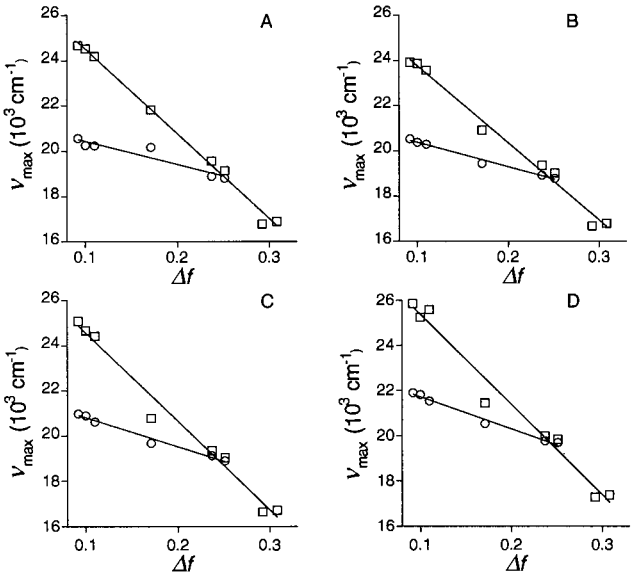

Figure 6. Lippert−Mataga plots for **1** (A), **2** (B), **3** (C), and **4** (D); ECT maxima are indicated by squares, CCT maxima by circles.

$$\nu_{CT} = \nu_{CT}(0) - \frac{2\mu_{CT}^2}{hc\rho^3}\Delta f = \nu_{CT}(0) - 10070\frac{\mu_{CT}^2}{\rho^3}\Delta f \quad (5)$$

$$\Delta f = \frac{(\epsilon_s - 1)}{(2\epsilon_s + 1)} - \frac{(n^2 - 1)}{(4n^2 + 2)} \quad (6)$$

In Figure 6, we have plotted the Franck−Condon maxima of both species versus Δf. As can be seen, the ECT and CCT data can be satisfactorily fitted by straight lines. Only the ECT values of **3** and **4** in di-*n*-pentyl ether (squares in Figure 6C,D at $\Delta f = 0.171$) deviate significantly. The slopes of the Lippert−Mataga plots for the ECT and CCT species are given in Table 4. The intercepts of both the ECT and CCT plots of **1**−**3** are nearly identical, indicating that the energies of the CT states are very similar in the three compounds. The higher intercepts for **4** are caused by the fact that the aniline electron donor is somewhat weaker than the 4-alkyl aniline donor incorporated in **1**−**3**.

TABLE 4: Experimental Parameters (10^3 cm^{-1}) for 1−4 Obtained from Lippert−Mataga Analysis

compd	$2\mu^2/hc\rho^3$ ECT	$\nu_{CT}(0)$ ECT	$2\mu^2/hc\rho^3$ CCT	$\nu_{CT}(0)$ CCT
1	37.5 ± 1.2	28.3 ± 0.3	10.3 ± 1.7	21.5 ± 0.3
2	34.2 ± 1.5	27.2 ± 0.3	10.9 ± 0.6	21.5 ± 0.1
3	39.3 ± 2.2	28.5 ± 0.5	12.8 ± 0.9	22.1 ± 0.1
4	40.0 ± 2.6	29.4 ± 0.5	14.2 ± 0.8	23.1 ± 0.1

TABLE 5: Radiative (k_f^{ECT}) and Nonradiative Decay Rates (Including Folding, $k_d^{ECT} + k_{fold}$) (10^6 s^{-1}) of the ECT Species in Solvents in which Harpooning Occurs

	1		**2**		**3**		**4**	
solvent	k_f^{ECT}	$k_d^{ECT} + k_{fold}$	k_f^{ECT}	$k_d^{ECT} + k_{fold}$	k_f^{ECT}	$k_d^{ECT} + k_{fold}$	k_f^{ECT}	$k_d^{ECT} + k_{fold}$
n-hexane	3.91	829	4.90	709				
cyclohexane	2.64	320	4.20	551	2.50	767	8.00	1658
trans-decalin	1.80	105	3.00	241				
di-*n*-pentyl ether	1.35	91	1.49	116	1.79	117		
benzene			1.33	157			1.04	184
diisopropyl ether	1.33	168	1.31	150	0.98	132		
diethyl ether	0.58	113	0.93	142	0.82	133		

TABLE 6: Product of the Quantum Yield of Folding and the Radiative Rate Constant (10^6 s^{-1}) for the CCT Species of 1−4 in Various Solvents

	1	**2**	**3**	**4**
solvent	$\Phi_{fold}k_f$	$\Phi_{fold}k_f$	$\Phi_{fold}k_f$	$\Phi_{fold}k_f$
n-hexane	1.87	2.59	1.68	
cyclohexane	2.66	2.30	2.87	4.80
trans-decalin	2.30	2.28		
di-*n*-pentyl ether	1.47	1.73	1.82	
benzene		1.39		1.21
diisopropyl ether	1.26	1.26	1.08	
diethyl ether	0.59	0.98	0.92	

TABLE 7: Franck−Condon Maxima (10^3 cm^{-1}), Decay Times (ns), and Contributions to the Total Quantum Yield of the Different Components of 1 in Methylcyclohexane at Various Temperatures

temperature (K)	ν_{ECT}	ν_{CCT}	τ_{ECT}	τ_{CCT}	A_{ECT}	A_{CCT}
298	23.7	20.3	1.9	23.0	0.063	0.937
278	23.8	20.3	3.3	23.5	0.090	0.910
258	23.8	20.3	6.2	24.3	0.155	0.845
238	23.8	20.2	11.4	25.5	0.475	0.525
218	23.7	20.1	21.7	27.7	0.533	0.467
178	24.3		5.5		0.511	
	23.9		19.1		0.489	
158	24.4		6.1		0.550	
	24.0		21.0		0.450	
138	24.3		5.9		0.527	
	24.1		19.8		0.473	

From the total fluorescence quantum yields (determined from the steady-state spectra[1]) and the SAS (obtained from the analysis of the streak data), we can now calculate the fractional quantum yields of the ECT species. For the CCT species, it is possible to determine the product of the fluorescence quantum yield and the quantum yield of folding ($\Phi_{total} = \Phi_{ECT} + \Phi_{fold}\Phi_{CCT}$). Unfortunately, the quantum yields of **4** have only been determined in a very limited polarity range.[2] Using the fractional quantum yields (Supporting Information, Table S5) and the corresponding decay times (Table 1), it is possible to calculate the radiative and nonradiative rate constants for the ECT species. For the CCT species, it is possible to calculate the product of the radiative rate constants and the quantum yields of folding.

Because we have no absolute way to determine the quantum yield of folding in the various solvents, we restrict ourselves to the study of the radiative and nonradiative rate constants of the ECT species. These are listed in Table 5. As is evident from Table 5, the radiative rate constant increases as the emission energy goes up (Table 3), which can be explained by an increased mixing of the charge-transfer state with the locally excited state of the acceptor,[15] a phenomenon observed before in similar systems.[16] The increase of the sum of the nonradiative and folding rate constants at high energy of the Franck−Condon maxima is much more pronounced. In this context, it should be realized that the folding process is expected to be the major relaxation pathway for the ECT species, and in the alkane solvents, a large driving force exists for this process. In Table 6, we give the product of the quantum yield of folding and the radiative rate constants for the CCT species. If we assume that the radiative rate constant, k_f^{CCT} is independent of the solvent, we can ascribe the decrease observed for the product $k_f^{CCT}\Phi_{fold}$ to a decrease of the quantum yield of folding upon increasing the polarity of the solvent. We should expect, however, that k_f^{CCT} will tend to decrease with increasing solvent polarity. Unfortunately, the two effects cannot be separated.

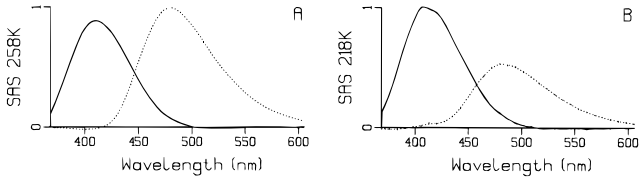

Figure 7. Species associated spectra (SAS) of **1** in methylcyclohexane at 258 K (left) and 218 K (right). Note that the second SAS plotted here is in fact the product of the quantum yield of folding and the true SAS of the CCT state.

3.2. Temperature Dependence of the Folding Process. For **1**, the temperature dependence of the fluorescence was studied in methylcyclohexane. At each temperature, the spectrotemporal parametrization method yields the contribution of both species to the total quantum yield. Furthermore, we also obtain the decay times of both species. In Figure 7, we show the SAS of the ECT and CCT species at two temperatures. We can nicely observe the relative increase of the ECT emission upon cooling, whereas also the corresponding ECT decay time increases considerably. Below 198 K, we observe two independently decaying components that possess almost identical emission band shapes but distinctively different decay times. All the Franck−Condon maxima, the decay times, and the contributions to the total quantum yield of the different components at the various temperatures are listed in Table 7.

When we estimate the Arrhenius activation barrier for the folding process using the decay times of the ECT species, we arrive at an activation barrier for **1** of ca. 6.1 kcal mol^{-1}, while Wegewijs[2] found a barrier of 3.6 kcal mol^{-1} for **4**. When using this approach, one must realize that by changing the temperature we also change both the dielectric constant and refractive index of the solvent as well as its viscosity. A detailed analysis of the individual contribution of these factors is not possible. Nevertheless, the significantly larger estimated Arrhenius activation barrier for **1** compared to that of **4**, shows that also the temperature-dependent measurements indicate that the introduction of the two alkyl tails effectively slows down the folding process.

4. Concluding Remarks

We have presented the fluorescence at room temperature of a set of harpooning compounds studied by the use of a streak camera system and analysis of the data by spectrotemporal parametrization. Thanks to the high information density and parallel multiwavelength acquisition realized by means of the

streak camera, which gives both time, intensity, and wavelength information, and the application of two-compartmental models to analyze the data, both the spectral changes and the kinetics could be studied in great detail. Previously, it had been assumed that the harpooning process can only occur in the gas phase[2] ($\epsilon_s = 1$) or in saturated hydrocarbon solvents ($\epsilon_s \approx 2$), but the present work clearly demonstrates that in the four compounds studied, harpooning occurs even in solvents with significantly higher dielectric permittivity (and thus stronger charge shielding) such as diethyl ether ($\epsilon_s = 4.34$). The ECT lifetimes for **4** are significantly shorter than those of the other harpooning systems, whereas those of **1** are the largest of all four studied systems. The monoalkyl compounds **2** and **3** show intermediate behavior. This indicates that the introduction of the long alkyl tails effectively slows down the rate of folding. The spectrotemporal parametrization method also yields the shapes of the emission spectra, enabling us to investigate the solvatochromic shifts by means of the Lippert−Mataga relation. As we unambiguously obtained the maxima of both the ECT and the CCT (in alkane and ether solvents) species in the nine solvents used, we could perform a much more accurate analysis than was possible in the past. Temperature-dependent measurements yielded the fluorescence maxima and the contribution to the total quantum yield of the ECT and CCT species and also provided the temperature-dependent decay times of both species, allowing an Arrhenius activation barrier of 6.1 kcal mol^{-1} to be determined for **1** in methylcyclohexane, which is distinctly higher than the barrier determined using the same approach for **4** (3.6 kcal mol^{-1}). It is expected that through the use of fluorescence measurements at different pressures and temperatures[13] a proper separation of the effects of viscosity and dielectric constant can be achieved.[17]

5. Experimental Section

The synthesis of the donor−acceptor compounds has been published before.[1]

Electronic absorption measurements were performed on a Hewlett-Packard 8453 diode array spectrometer. The time-resolved fluorescence measurements were performed using a Hamamatsu streak camera system, consisting of a Chromex IS250 spectrograph, an M5677 slow-speed sweep unit, a C4792 trigger unit, a C5680 blanking unit, and a C4742−95 digital CCD camera. For excitation, an LTB MSG400 nitrogen laser (337 nm, fwhm $\approx$ 0.5 ns) operating at 50 Hz was used to pump a UDL 210 dye laser (Rhodamin B in ethanol), resulting after frequency doubling in ca. 310 nm pulses (fwhm$\approx$0.5 ns). In the analysis of the streak data, the instrument response was modeled with a Gaussian time profile. For the measurements at room temperature, the excitation and emission light were fiber-coupled to the spectrograph; in the low-temperature measurements a lens was used to image the fluorescence light onto the entrance slit of the spectrograph.

The images consist of 512 $\times$ 512 pixels. In the time direction, the resolution is limited by the width of the excitation pulse (ca. 500 ps fwhm) and by the pointspread function of the imaging device. Thus, the Gaussian-shaped fwhm of the instrument response depends on the time base used. It varied from 0.5 to 5 ns fwhm. In the wavelength direction, the resolution is limited by the slit and the grating used and was ca. 6 nm fwhm. Because the emission bands are broad and structureless, we reduced the amount of data points for the analysis by summing the response over 11−13 pixels (depending on the spectral window used), which effectively is a smoothing over ca. 7−8 nm. Thus, a data set of 512 $\times$ 33 points was routinely used in the further analysis.

Commercially available spectrograde solvents were used. When the purity of the solvent was found to be insufficient, the solvent was purified by standard procedures.[18] All alkyl ethers were distilled from CaH_2 or $LiAlH_4$ prior to use. Ethyl acetate was washed with a saturated sodium carbonate solution and distilled from CaH_2. The samples were degassed by at least four freeze−pump−thaw cycles or by purging with argon for 15 min.

Acknowledgment. This research was supported (in part) by The Netherlands Foundation for Chemical Research (SON) with financial aid from The Netherlands Organization for the Advancement of Research (NWO)

Supporting Information Available: Tables S1−S4 presenting the estimated fluorescence spectral parameters for **1**−**4** in the solvents used and Table S5 reporting quantum yield data (5 pages). Ordering information is given on any current masthead page.

References and Notes

(1) Lauteslager, X. Y.; Bartels, M. J.; Piet, J. J.; Warman, J. M.; Verhoeven, J. W.; Brouwer, A. M. *Eur. J. Org. Chem.* **1998**, 2467−2481.

(2) (a) Wegewijs, B.; Hermant, R. M.; Verhoeven, J. W.; Kunst, A. G. M.; Rettschnick, R. P. H. *Chem. Phys. Lett.* **1987**, *140*, 587. (b) Wegewijs, B. Long-range charge separation in solvent-free donor-bridge-acceptor systems. Donor-bridge-acceptor molecules in splendid isolation, Ph.D. Thesis, University of Amsterdam, 1994.

(3) van Stokkum, I. H. M.; Brouwer, A. M.; van Ramesdonk, H. J.; Scherer, T. *Proc. Kon. Ned. Akad. Wet.* **1993**, *96*, 43.

(4) van Stokkum, I. H. M.; Scherer, T.; Brouwer, A. M.; Verhoeven, J. W. *J. Phys. Chem.* **1994**, *98*, 852.

(5) Scherer, T.; van Stokkum, I. H. M.; Brouwer, A. M.; Verhoeven, J. W. *J. Phys. Chem.* **1994**, *98*, 10539.

(6) (a) Anderson, D. H. *Compartmental modeling and tracer kinetics*; Springer: Berlin, 1983. (b) Godfrey, K. *Compartmental models and their applications*; Academic Press: London, 1983.

(7) Lakowicz, J. R. *Principles of fluorescence spectroscopy*; Plenum Press: New York, 1983. Förster, T. *Fluoreszenz Organischer Verbindimgen*; Vandenhoeck & Ruprecht: Söttinger, 1951; p 17. According to this source, the multiplication by λ^2 is superfluous. This will have a minor effect on the estimated spectral parameters and will not affect any of the conclusions drawn from the current analysis.

(8) (a) Fraser, R. D. B.; Suzuki, E. *Anal. Chem.* **1969**, *41*, 37. (b) Sevilla, J. M.; Dominguez, M.; Garcia-Blanco, F.; Blazquez, M. *Comput. Chem.* **1989**, *13*, 197.

(9) Marcus, R. A. *J. Phys. Chem.* **1989**, *93*, 3078.

(10) Reynolds, L.; Gardecki, J. A.; Frankland, S. J. V.; Horng, M. L.; Maroncelli, M. *J. Phys. Chem.* **1996**, *100*, 10337.

(11) (a) Squillacote, M. E.; Sheridan, R. S.; Chapman, O. L.; Anet, F. A. L. *J. Am. Chem. Soc.* **1975**, *97*, 3244. (b) Dixon, D. A.; Komornicki, A. *J. Phys. Chem.* **1990**, *94*, 5630.

(12) Brunschwig, B. S.; Ehrenson, S.; Sutin, N. *J. Phys. Chem.* **1987**, *91*, 4714.

(13) Schneider, S.; Jäger, W.; Lauteslager, X. Y.; Verhoeven, J. W. *J. Phys. Chem.* **1996**, *100*, 8118.

(14) (a) Lippert, E. *Z. Naturforsch A* **1955**, *10A*, 541. (b) Lippert, E. *Z. Elektrochem., Ber. Bunsen-Ges. Physik. Chem.* **1957**, *61*, 962. (c) Mataga, N.; Kaifa, Y.; Koizumi, M. *Bull. Chem. Soc. Jpn.* **1955**, *28*, 690. (d) Mataga, N.; Kaifa, Y.; Koizumi, M. *Bull. Chem. Soc. Jpn.* **1955**, *29*, 465.

(15) Bixon, M.; Jortner J.; Verhoeven, J. W. *J. Am. Chem. Soc.* **1994**, *116*, 7349.

(16) (a) Scherer, T. Conformational dynamics of fluorescent exciplexes. On the structure of the emissive state in bridged donor−acceptor systems, Ph.D. Thesis, University of Amsterdam, 1994. (b) Willemse, R. J. Photoinduced electron transfer in donor−acceptor systems with redox-active bridges, Ph.D. Thesis, University of Amsterdam, 1997.

(17) Bleisteiner, B.; Schneider, S.; Lauteslager, X. Y.; Verhoeven, J. W.; Brouwer, A. M. To be published.

(18) *Purification of Laboratory Chemicals*, 2nd ed.; Perrin, D. D., Armarego, W. L. F., Perrin, D. R., Ed.; Pergamon Press Ltd.: Oxford, 1980.